Progress In Electromagnetics Research, Vol. 173, 1–8, 2022

An Ultra-Thin Wideband Reflection Reduction Metasurface Based on Polarization Conversion

Tiancheng Han*, Kaihuai Wen, Zixuan Xie, and Xiuli Yue

Abstract—Reflection reduction metasurface is capable of suppressing the radar cross section of a target, which is of great importance in stealth technology. However, it is still a challenge to realize broadband and low-profile simultaneously within a simple design. Here, we experimentally demonstrate an ultra-thin wideband reflection reduction metasurface, which is achieved by utilizing polarization conversion instead of resonant absorption. The simple cut-wire unit cell is adopted to perform efficient cross polarization conversion, which leads to a polarization conversion ratio above 90% ranging from 8.4 to 14.7 GHz. By arranging the 0/1 units in chessboard layout, the reflection reduction reaches 10 dB from 8.1 GHz to 14.6 GHz. Measured results agree well with simulated ones, which validates the effectiveness of the proposed structure. The ratio of thickness to maximum wavelength reaches 0.56 while the relative bandwidth reaches 57.3%, demonstrating an excellent comprehensive performance. Since our structure consists of refractory ceramic materials, it is promising for radar cross section reduction in high temperature environment.

1. INTRODUCTION

Suppressing the radar cross section (RCS) of a target is of great importance in stealth technology. Owing to the good compatibility and universality of radar absorbing materials (RAMs), they have been successfully used for the RCS reduction of various targets. Compared to dielectric RAMs with low efficiency absorption [1] or large thickness [2], magnetic RAMs may obtain better impedance match, showing a strong absorption with a thin thickness [3]. Contemporary aircrafts, possessing high-invisibility and high-speed simultaneously, requires heat-resisting RAMs that have stable stealth performance in a wide temperature range. The magnetic RAMs are invalid at high temperature since their magnetic response gradually deteriorates with temperature rising and completely disappears above Curie temperature.

Emerging metamaterial [4] and metasurface [5] have been attracting much attention due to their great capability on controlling the propagation of electromagnetic (EM) waves, thus leading to a great deal of unprecedented devices, e.g., absorbing metamaterials [6, 7] and coding metamaterials [8, 9]. Absorbing metamaterials have been designed to meet high temperature environment by utilizing single layer frequency selective surface (FSS) [10, 11] and double layer FSS [12]. However, high loss is required in the top metal layer or the middle dielectric layer, resulting in a large thickness [13], or a narrow bandwidth [10]. Different from absorbing metamaterials based on amplitude regulation, coding metamaterials, which are based on phase regulation, can redirect scattered energy into non-mirror direction, hence suppressing the strong specular reflection [14]. Since magnetic materials are not required, the reflection reduction metasurface is promising for the application in high temperature environment [15]. An all-dielectric heat-resisting metasurface composed of patterned aluminum nitride

Received 14 December 2021, Accepted 2 February 2022, Scheduled 8 February 2022

* Corresponding author: Tiancheng Han (tchan@uestc.edu.cn).

The authors are with the National Engineering Research Center of Electromagnetic Radiation Control Materials, State Key Laboratory of Electronic Thin Film and Integrated Devices, University of Electronic Science and Technology of China, Chengdu 610054, China.

ceramics has been designed to achieve specular reflection reduction, which cannot meet the mechanical requirements in practice [16]. In contrast, an all-metallic heat-resisting metasurface working in $8 \sim 17$ GHz has also been designed to achieve specular reflection reduction with a thickness of 9 mm [17].

By using anisotropic unit cell, polarization converters can change the polarization direction of reflected or transmitted electric field, which has been attracting much attention in recent years. Polarization convertors have been proposed with single-band [18], dual-bands [19, 20], multi-bands [21], and broadband [22–25]. To further expand the bandwidth, many kinds of different unit cells, such as ring/disk cavity [22], elliptical disk-ring [24], and double-head arrow [25], have been reported. In addition, multilayered metasurface may achieve broadband polarization conversion, which however suffers from complicated fabrication and large thickness [26]. Take the polarization conversion unit as element "0" and rotate it 90° to be element "1". The two elements can be arranged in a manner of chessboard [27–29] or random [30, 31] layout to achieve broadband specular reflection reduction. However, it is still a challenge so far to realize broadband and low-profile simultaneously within a simple design.

Here, we demonstrate an ultra-thin wideband reflection reduction metasurface based on polarization conversion. The proposed structure is metal-dielectric-metal, in which the metal is silver, and the dielectric is alumina ceramic. The unit cell is capable of effectively converting linearly polarized waves into cross-polarized waves with polarization conversion ratio (PCR) above 90% from 8.4 to 14.7 GHz. By arranging the 0/1 units in chessboard layout, a reflection reduction of 10 dB is achieved in the frequency of 8.1–14.6 GHz. Experimental results show a good agreement with simulated ones, which validates our design. Compared to the reported results [28–30, 32–34], our design demonstrates a thinner thickness and wider bandwidth.

2. DESIGN, SIMULATION AND ANALYSIS

A polarization converter is a periodic array of metal-dielectric-metal unit cells, in which the unit cell is generally anisotropic [35]. Without losing generality, cut-wire is chosen as the unit cell due to its easy fabrication and huge anisotropy [36, 37]. Figure 1(a) shows the working principle of the proposed design, in which the normally incident waves are scattered into four beams far away from the specular direction, thus achieving an efficiently specular reflection reduction. Both top metasurface and bottom

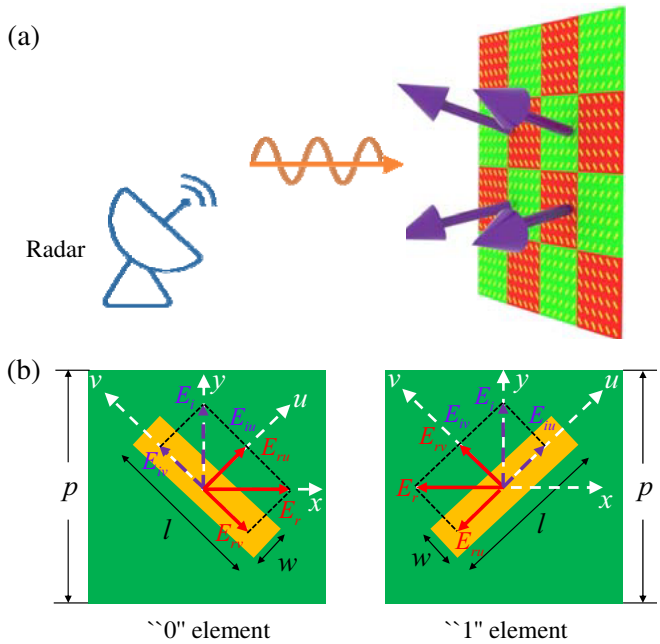

Figure 1. (a) Scheme of the proposed design with efficiently specular reflection reduction. (b) The working principle of polarization conversion and reflection reduction of "0" element and "1" element.

reflector are silver. The dielectric spacer is alumina ceramic with permittivity of 9.7 and loss tangent of 0.017. Based on genetic algorithm of CST Microwave Studio, the optimal geometric parameters are obtained as $l = 4.78\,\text{mm}$, $w = 1.42\,\text{mm}$, and $p = 7.5\,\text{mm}$. It is worth mentioning that the total thickness of the polarization converter is 2 mm.

Figure 1(b) shows the working principle of element "0" and element "1". We consider a normally incident EM wave polarized along the y-direction, and the electric field can be expressed as $\vec{E}_i = (\hat{u}E_{iu} + \hat{v}E_{iv})e^{j\varphi}$. Here, u-v coordinate system is obtained by rotating the x-y coordinate system counterclockwise 45°. Accordingly, the electric field of the reflected waves is obtained as $\vec{E}_r = (\hat{u}E_{iu}|r_u|e^{j\varphi_u} + \hat{v}E_{iv}|r_v|e^{j\varphi_v})e^{j\varphi}$, where $|r_u|$ and $|r_v|$ represent the amplitudes of reflection coefficients, and φ_u and φ_v represent the phases of reflection coefficients. Due to the anisotropic property of the unit cell, there is a phase difference ($\Delta\varphi = |\varphi_u - \varphi_v|$). If $|r_u| = |r_v|$ and $\Delta\varphi = 180°$, the reflected electric field is polarized along the x-direction. In other words, the oscillation direction of the incident electric field has been rotated by 90°. When element "0" is rotated 90° clockwise, element "1" is obtained. The phase difference of the reflected electric field of element "0" and element "1" is 180°, thus achieving reflection reduction.

Figures 2(a) and 2(b) show the amplitudes and phases of the reflection coefficients, respectively. Strong reflection can be found for both components in the whole frequency band, and a phase difference within the range $180° \pm 37°$ is obtained from 8.4 to 14.7 GHz, thus leading to a high efficiency and broadband polarization conversion. Figure 2(c) shows the co-polarized ($|r_{yy}|$) and cross-polarized ($|r_{xy}|$) reflection amplitudes. We can see that a strong cross-polarization ($|r_{xy}|$) is obtained in the frequency range of 8.4 to 14.7 GHz. To evaluate the efficiency of polarization conversion, we calculate the polarization conversion ratio (PCR) that is defined as $\text{PCR} = |r_{xy}|^2/(|r_{xy}|^2 + |r_{yy}|^2)$. As shown in Figure 2(d), the PCR is higher than 90% from 8.4 to 14.7 GHz. Especially, the PCR reaches 100% at 9 GHz, 11.3 GHz, and 14.3 GHz, which implies a perfect polarization conversion.

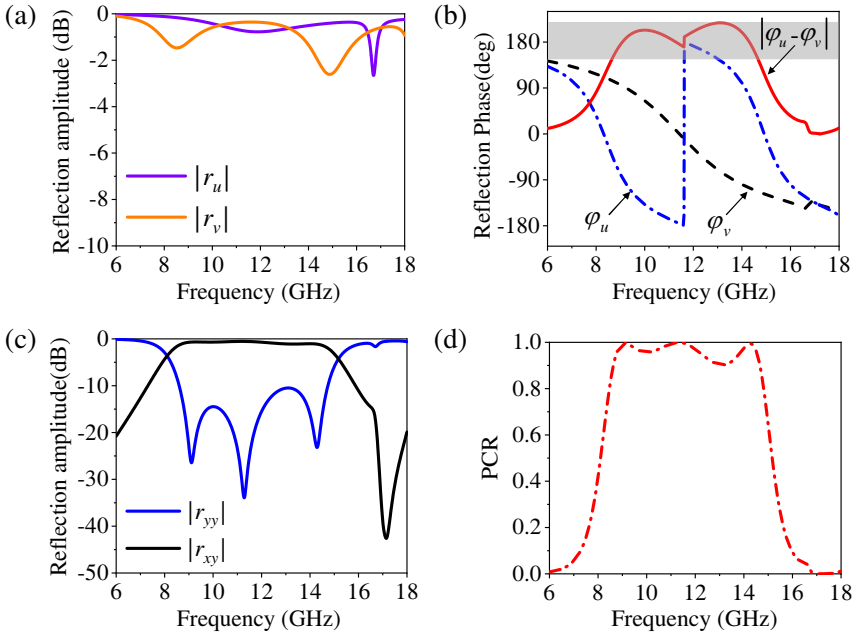

Figure 2. (a) Amplitude of the reflection coefficients. (b) Phase of the reflection coefficients. (c) Co-polarized ($|r_{yy}|$) and cross-polarized ($|r_{xy}|$) reflection amplitude. (d) The calculated PCR.

From Figure 2(a) we can see that the reflection is not 100%, which implies an absorption since no transmission occurs. To find out, we examine two cases, i.e., the dielectric spacer is lossless and lossy, respectively. By calculating the reflection of the structure with and without dielectric loss, it is found that the reflection is 100% in the whole spectrum when the dielectric spacer is lossless. In contrast, absorption appears when the dielectric spacer is lossy. Therefore, the absorption observed in Figure 2(a)

is attributed to the loss of the dielectric spacer.

To understand the physical mechanism, the surface currents on the top metasurface and bottom metal plate are simulated at 9 GHz, 11.3 GHz, and 14.3 GHz, respectively, as shown in Figure 3. We can see that the surface currents on the top layer are opposite to those on the bottom layer at 9 GHz and 11.3 GHz, which is known as magnetic resonance. In contrast, they are parallel to each other at 14.3 GHz, which is known as electric resonance. The superposition of the three resonances leads to a high-efficiency and broadband polarization conversion.

To interpret the perfect polarization conversion at the three resonant frequencies, the magnetic/electric field is decomposed as illustrated in Figure 3. From Figure 3(a) we can see that a π phase difference is generated between H_{ru} and H_{iu}, while H_{rv} keeps in phase relative to H_{iv}, which makes the reflected magnetic field rotate 90°. In Figure 3(b), a π phase difference is generated between H_{rv} and H_{iv}, while H_{ru} keeps in phase relative to H_{iu}, which also makes the reflected magnetic field rotate 90°. In Figure 3(c), a π phase difference is generated between E_{iv} and E_{rv}, while E_{ru} keeps in phase relative to E_{iu}, which makes the reflected electric field rotate 90°. Broadband polarization conversion is achieved by the superposition of the three resonances.

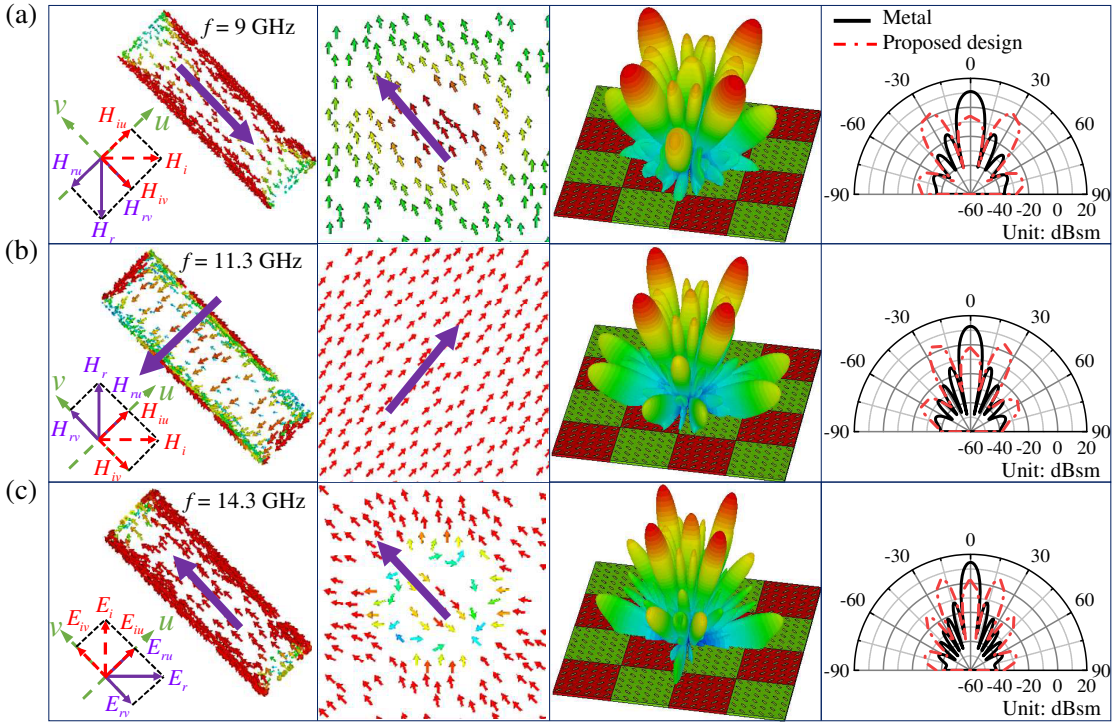

Figure 3. Surface current distributions on the top metasurface (first column), surface current distributions on the bottom metal plate (second column), 3D scattering patterns (third column), and 2D scattering patterns at $\varphi = 45°$ plane (fourth column) at different resonance frequencies. (a) 9 GHz. (b) 11.3 GHz. (c) 14.3 GHz.

By arranging element "0" and element "1" in chessboard layout, we derive a reflection reduction structure, which scatters the incident wave into four main beams deviating from the specular reflection. For a metasurface with $N \times N$ elements, in which each element contains a subarray of "0" or "1" lattices, the scattered far-field can be given as:

$$f(\theta,\phi) = f_e(\theta,\phi) \sum_{m=1}^{N} \sum_{n=1}^{N} \exp\left\{-i\phi(m,n) - ikD\sin\theta\left[\left(m-\frac{1}{2}\right)\cos\phi + \left(n-\frac{1}{2}\right)\sin\phi\right]\right\} \quad (1)$$

where θ and ϕ are the elevation and azimuth angles of an arbitrary direction, respectively; D is the

dimension of each element satisfying $D = np$, here $n = 6$; $\phi(m, n)$ is the scattering phase of the lattice, which is either 0 or 180°; $f_e(\theta, \phi)$ represents the scattering field of each lattice; k is the wave vector in free space. The third column and fourth column of Figure 3 respectively show the 3D scattering patterns and 2D scattering patterns at $\varphi = 45°$ plane at different resonance frequencies, from which we can see that the specular reflection is reduced significantly.

3. FABRICATION AND EXPERIMENT

The experiment setup is schematically demonstrated in Figure 4(a), in which a pair of broadband horn antennas (one is transmitter, and the other is receiver) working in 2–18 GHz are connected to a Vector Network Analyzer (Agilent 8720ET) to measure the reflectivity of the structure. We fabricated a

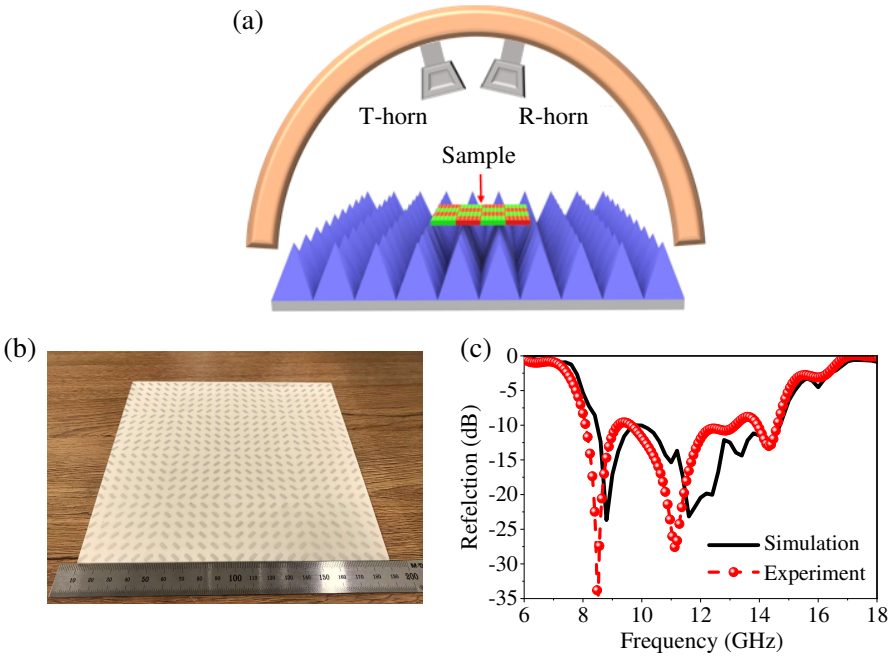

Figure 4. (a) Schematic diagram of the experiment setup. (b) Photograph of the fabricated sample. (c) Measured and simulated results.

Table 1. Comparison with other reflection reduction metasurface.

Ref.	OB* (GHz)	RB* (%)	d (mm)	d/λ_l
[27]	10.2–19.3	61.7	3	0.102
[28]	8.2–13.8	51	3.5	0.096
[29]	10.42–18.12	54	2.6	0.090
[30]	7.6–11.3	39	2.6	0.066
[32]	11–15	30.8	4	0.147
[33]	5.6–7	41.3	3.5	0.065
[34]	5.2–5.8	10.9	3	0.055
[38]	86.4–93.2	7.6	1.27	0.366
Present study	8.1–14.6	57.3	2	0.056

d: the thickness of the structure, λ_l: wavelength corresponding to the lowest frequency, OB: operating band (Reflection < -10 dB), RB: relative bandwidth (Reflection < -10 dB).

180 mm × 180 mm × 2 mm sample that is composed of 6 × 6 equal-sized lattices based on screen-printing technology. First, a 300-mesh screen was used to print the metasurface pattern on one side of alumina ceramic. Second, the sample was heated to 90°C in an oven and held for 10 minutes. Finally, an alumina foil with a thickness of 0.06 mm was affixed at the other side of alumina ceramic. Figure 4(b) shows a photo of the fabricated sample. Figure 4(c) shows the measured and simulated reflections of the structure, which demonstrate a good agreement. Specifically, simulation result shows a reflection below −10 dB from 8.4 GHz to 14.7 GHz (with an average reflection of −14.13 dB), and measured result shows a reflection below −10 dB from 8.1 GHz to 14.6 GHz (with an average reflection of −13.82 dB). The little difference is attributed to the fabrication tolerance.

Compared with the previous designs, our scheme demonstrates a better performance, as shown in Table 1. The total thickness of our structure is only 2 mm, which is thinner than most reported structures [27–30, 32–34]. Compared to the structures with wider bandwidth [27] or thinner thickness [38], our structure possesses a relative bandwidth of 57.3%, and the ratio of thickness to maximum wavelength reaches 0.056, demonstrating an excellent comprehensive performance.

4. CONCLUSION

In summary, we have designed, fabricated, and measured an ultra-thin wideband reflection reduction metasurface, which is achieved by utilizing polarization conversion instead of resonant absorption. Experimental results show that a −10 dB specular reflection is achieved from 8.1 GHz to 14.6 GHz, which agrees well with the simulated results. The ratio of thickness to maximum wavelength reaches 0.056 while the relative bandwidth reaches 57.3%, demonstrating an excellent comprehensive performance. Compared to the traditional metasurfaces that can only work at room temperature, our structure can be applied to high-temperature environment. The proposed scheme can be further extended to the manipulation of photonics [39].

REFERENCES

1. Pang, Y., Y. Li, J. Wang, M. Yan, S. Qu, S. Xia, and Z. Xu, "Electromagnetic reflection reduction of carbon composite materials mediated by collaborative mechanisms," *Carbon*, Vol. 147, 112–119, 2019.
2. Zhang, Y., Y. Huang, T. Zhang, H. Chang, P. Xiao, H. Chen, Z. Huang, and Y. Chen, "Broadband and tunable high-performance microwave absorption of an ultralight and highly compressible graphene foam," *Advanced Materials*, Vol. 27, 2049–2053, 2015.
3. Rozanov, K. N., "Ultimate thickness to bandwidth ratio of radar absorbers," *IEEE Transactions on Antennas and Propagation*, Vol. 48, 1230–1234, 2000.
4. Lee, D., S. So, G. Hu, M. Kim, T. Badloe, H. Cho, J. Kim, H. Kim, C. Qiu, and J. Rho, "Hyperbolic metamaterials: Fusing artificial structures to natural 2D materials," *eLight*, Vol. 2, 1, 2022.
5. Yu, N., P. Genevet, M. Kats, F. Aieta, J. Tetienne, F. Capasso, and Z. Gaburro, "Light propagation with phase discontinuities: Generalized laws ofreflection and refraction," *Science*, Vol. 334, 333–337, 2011.
6. Landy, N. I., S. Sajuyigbe, J. J. Mock, D. R. Smith, and W. J. Padilla, "Perfect metamaterial absorber," *Physical Review Letters*, Vol. 100, 207402, 2008.
7. Yu, P., L. V. Besteiro, Y. Huang, J. Wu, L. Fu, H. H. Tan, C. Jagadish, G. P. Wiederrecht, A. O. Govorov, and Z. Wang, "Broadband metamaterial absorbers," *Advanced Optical Materials*, Vol. 7, 1800995, 2019.
8. Cui, T., M. Qi, X. Wan, J. Zhao, and Q. Cheng, "Coding metamaterials, digital metamaterials and programmable metamaterials," *Light: Science & Application*, Vol. 3, e218, 2014.
9. Liang, L., M. Qi, J. Yang, X. Shen, J. Zhai, W. Xu, B. Jin, W. Liu, Y. Feng, C. Zhang, H. Lu, H. Chen, L. Kang, W. Xu, J. Chen, T. Cui, P. Wu, and S. Liu, "Anomalous terahertz reflection and scattering by flexible and conformal coding metamaterials," *Advanced Optical Materials*, Vol. 3, 1374–1380, 2015.

10. Li, Y., W. Li, Y. Wang, J. Cao, and J. Guan, "Refractory metamaterial microwave absorber with strong absorption insensitive to temperature," *Advanced Optical Materials*, Vol. 6, 1800691, 2018.
11. Shao, T., H. Ma, J. Wang, M. Yan, M. Feng, Z. Yang, Q. Zhou, J. Wang, Y. Meng, S. Zhao, and S. Qu, "Ultra-thin and high temperature NiCrAlY alloy metamaterial enhanced radar absorbing coating," *Journal of Alloys and Compounds*, Vol. 832, 154945, 2020.
12. Yang, Z., F. Luo, W. Zhou, H. Jia, and D. Zhu, "Design of a thin and broadband microwave absorber using double layer frequency selective surface," *Journal of Alloys and Compounds*, Vol. 699, 534–539, 2017.
13. Tian, H., H. Liu, and H. Cheng, "A high-temperature radar absorbing structure: Design, fabrication, and characterization," *Composites Science and Technology*, Vol. 90, 202–208, 2014.
14. Chen, J., Q. Cheng, J. Zhao, D. S. Dong, and T.-J. Cui, "Reduction of radar cross section based on a metasurface," *Progress In Electromagnetics Research*, Vol. 146, 71–76, 2014.
15. Zhou, Y., Y. Yang, J. Xie, H. Chen, G. Zhang, F. Li, L. Zhang, X. Wang, X. Weng, P. Zhou, and L. Deng, "Broadband RCS reduction for electrically-large open-ended cavity using random coding metasurfaces," *Journal of Physics D: Applied Physics*, Vol. 52, 315–303, 2019.
16. Sun, L., X. Wang, Z. Yu, J. Huang, and L. Deng, "Patterned AlN ceramic for high-temperature broadband reflection reduction," *Journal of Physics D: Applied Physics*, Vol. 52, 235102, 2019.
17. Xie, X., M. Pu, Y. Huang, X. Ma, X. Li, Y. Guo, and X. Luo, "Heat resisting metallic meta-skin for simultaneous microwave broadband scattering and infrared invisibility based on catenary optical field," *Advanced Materials Technologies*, Vol. 4, 1800612, 2019.
18. Hao, J., Y. Yuan, L. Ran, T. Jiang, J. A. Kong, C. T. Chan, and L. Zhou, "Manipulating electromagnetic wave polarizations by anisotropic metamaterials," *Physical Review Letters*, Vol. 99, 063908, 2007.
19. Li, F., L. Zhang, P. Zhou, H. Chen, R. Zhao, Y. Zhou, D. Liang, H. Lu, and L. Deng, "Dual-band reflective polarization converter based on slotted wire resonators," *Applied Physics B: Lasers and Optics*, Vol. 124, 28, 2018.
20. Nama, L., Nilotpal, S. Bhattacharyya, and P. K. Jain, "A metasurface-based, ultrathin, dual-band, linear-to-circular, reflective polarization converter," *IEEE Antennas and Propagation Magazine*, Vol. 63, 100–110, 2021.
21. Huang, X., D. Yang, and H. Yang, "Multiple-band reflective polarization converter using U-shaped metamaterial," *Journal of Applied Physics*, Vol. 115, 103505, 2014.
22. Shi, H., J. Li, A. Zhang, J. Wang, and Z. Xu, "Broadband cross polarization converter using plasmon hybridizations in a ring/disk cavity," *Optics Express*, Vol. 22, 20973–20981, 2014.
23. Loncar, J., A. Grbic, and S. Hrabar, "A reflective polarization converting metasurface at X-band frequencies," *IEEE Transactions on Antennas and Propagation*, Vol. 66, 3213–3218, 2018.
24. Lin, B., B. Wang, W. Meng, X. Da, W. Li, Y. Fang, and Z. Zhu, "Dual-band high-efficiency polarization converter using an anisotropic metasurface," *Journal of Applied Physics*, Vol. 119, 183103, 2016.
25. Chen, H., J. Wang, H. Ma, S. Qu, Z. Xu, A. Zhang, M. Yan, and Y. Li, "Ultra-wideband polarization conversion metasurfaces based on multiple plasmon resonances," *Journal of Applied Physics*, Vol. 115, 154504, 2014.
26. Jia, Y., Y. Liu, W. Zhang, and S. Gong, "Ultra-wideband and high-efficiency polarization rotator based on metasurface," *Applied Physics Letters*, Vol. 109, 051901, 2016.
27. Jiang, W., Y. Xue, and S.-X. Gong, "Polarization conversion metasurface for broadband radar cross section reduction," *Progress In Electromagnetics Research Letters*, Vol. 62, 9–15, 2016.
28. Jia, Y., Y. Liu, Y. J. Guo, K. Li, and S. Gong, "Broadband polarization rotation reflective surfaces and their applications to RCS reduction," *IEEE Transactions on Antennas and Propagation*, Vol. 64, 179–188, 2016.
29. Long, M., W. Jiang, and S. Gong, "Wideband RCS reduction using polarization conversion metasurface and partially reflecting surface," *IEEE Antennas Wireless and Propagation Letters*, Vol. 16, 2534, 2017.

30. Khalaj-Amirhosseini, M. and M. Khanjarian, "Radar cross section reduction using polarization cancellation approach," *Progress In Electromagnetics Research Letters*, Vol. 74, 107–110, 2018.
31. Al-Nuaimi, M. K. T., W. Hong, and Y. He, "Design of diffusive modified chessboard metasurface," *IEEE Antennas Wireless and Propagation Letters*, Vol, 18, 1621–1625, 2019.
32. Zhou, Y., X. Cao, J. Gao, H. Yang, and S. Li, "Reconfigurable metasurface for multiple functions: Magnitude, polarization and phase modulation," *Optics Express*, Vol. 26, 29451–29459, 2018.
33. Yang, J., Y. Cheng, D. Qi, and R. Gong, "Study of energy scattering relation and RCS reduction characteristic of matrix-type coding metasurface," *Applied Sciences-Basel*, Vol. 8, 1231, 2018.
34. Liu, Y., Y. Jia, W. Zhang, and F. Li, "Wideband RCS reduction of a slot array antenna using a hybrid metasurface," *IEEE Transactions on Antennas and Propagation*, Vol. 68, 3644–3652, 2020.
35. Xu, J., R. Li, S. Wang, and T. Han, "Ultra-broadband linear polarization converter based on anisotropic metasurface," *Optics Express*, Vol. 26, 26235–26241, 2018.
36. Hu, C., X. Li, Q. Feng, X. Chen, and X. Luo, "Investigation on the role of the dielectric loss in metamaterial absorber," *Optics Express*, Vol. 18, 6598–6603, 2010.
37. Zhang, L., S. Liu, L. Li, and T. Cui, "Spin-controlled multiple pencil beams and vortex beams with different polarizations generated by pancharatnam-berry coding metasurfaces," *ACS Applied Materials & Interfaces*, Vol. 9, 36447–36455, 2017.
38. Al-Nuaimi, M. K. T., Y. He, and W. Hong, "Design of 1-bit coding engineered reflectors for EM-wave shaping and RCS modifications," *IEEE Access*, Vol. 6, 75422–75428, 2018.
39. Chen, Z. and, M. Segev, "Highlighting photonics: Looking into the next decade," *eLight*, Vol. 1, 2, 2021.